Copy
RM E56J18

RESEARCH MEMORANDUM

INTERNAL PERFORMANCE OF SEVERAL AUXILIARY AIR INLETS IMMERSED IN A TURBULENT BOUNDARY LAYER AT MACH NUMBERS OF 1.3, 1.5, AND 2.0

By Ronald G. Huff and Arthur R. Anderson

Lewis Flight Propulsion Laboratory
Cleveland, Ohio

NATIONAL ADVISORY COMMITTEE
FOR AERONAUTICS

WASHINGTON
January 18, 1957

NACA RM E56J18

NATIONAL ADVISORY COMMITTEE FOR AERONAUTICS

RESEARCH MEMORANDUM

INTERNAL PERFORMANCE OF SEVERAL AUXILIARY AIR INLETS IMMERSED IN A TURBULENT BOUNDARY LAYER AT MACH NUMBERS OF 1.3, 1.5, AND 2.0

By Ronald G. Huff and Arthur R. Anderson

SUMMARY

An experimental investigation of nine full-scale auxiliary air inlets immersed in a turbulent boundary layer was conducted at Mach numbers of 1.3, 1.5, and 2.0. Rectangular inlets with a turning angle of 10° and rectangular and circular inlets without turning were tested. Also included were external-compression and simple-scoop inlets.

Inlet pressure recovery and mass-flow ratios for various amounts of immersion in the boundary layer were compared with theoretical predictions. Recoveries varied from about 95 percent of theoretical in the free stream to 80 percent with the inlets fully immersed, while the corresponding mass flows were usually above 95 percent of theoretical. A simple calculation based on a stream-filament method proved to be an adequate approximation to more exact theoretical solutions.

Turning the flow 10° before diffusion resulted in pressure-recovery losses of 0.03 and 0.07. External compression did not improve the pressure recovery at critical operation over that of a normal-shock inlet. Total-pressure distortions at the diffuser exit with critical inlet operation were usually under 5 percent.

INTRODUCTION

Auxiliary air intakes find application in supplying secondary air for ejector nozzles as well as air for accessory equipment. In either application it is necessary that the air handling characteristics of the inlets be matched to the requirements of the components they supply. References 1 and 2, for example, illustrate the inlet-ejector matching problem. It is shown in reference 1 that drag reductions may frequently be realized by immersing the auxiliary inlet in the boundary layer.

Previous research has yielded some information on the performance of auxiliary inlets in a turbulent boundary layer. The performance of rectangular inlets with turning (refs. 2 and 3) and circular inlets without turning (ref. 4) has been reported. In addition, the performance of boundary-layer removal systems under main air inlets is often a source of auxiliary-inlet data. A systematic investigation was deemed necessary, however, to determine more fully the effect of flow turning, inlet shape, and external compression on auxiliary-inlet performance in a turbulent boundary layer. The results of such an investigation conducted in the 8- by 6-foot supersonic wind tunnel of the NACA Lewis laboratory are reported herein.

SYMBOLS

The following symbols are used in this report:

A	area
a	width of rectangular inlet (fig. 1)
b	height of rectangular inlet
D	diffuser-exit inside diameter
d	diameter of circular inlet
I	distance measured from edge of boundary layer to point on inlet lip closest to generating surface
$\overline{I}$	distance measured from edge of boundary layer to centroid of inlet (positive within boundary layer (fig. 1))
L	length of conical portion of diffuser
l	length of inlet constant-area section
M	Mach number
m/m_0	ratio of mass flow in duct to mass flow passing through equal area in free stream
P	total pressure
$\frac{\Delta P}{P_{av}}$	distortion parameter, difference between highest and lowest total pressure divided by average total pressure

T	total temperature
U_0	velocity in free stream
u	velocity in boundary layer
w	weight flow, (lb/sec)/sq ft
w_c	corrected weight flow, $w\sqrt{\frac{T}{519}}\Big/\frac{P}{2116}A_4$, (lb/sec)/sq ft
Y	normal distance measured from boundary-layer generating surface
β	conical diffuser included angle
δ	boundary-layer thickness
Ω	flow turning angle

Subscripts:

0	free-stream conditions
1,2,3,4	inlet stations (fig. 1)

APPARATUS AND PROCEDURE

This experiment essentially extends the work of reference 4 to include nine additional inlet configurations of varying shape and turning angle. Test Mach numbers were 1.3, 1.5, and 2.0, and immersion ratios I/δ were 1.0, 0.46, and free stream. The free-stream Reynolds number per foot varied from 5.25×10^6 to 4.30×10^6 over the Mach number range. In all other respects, the apparatus and procedure were essentially the same as in the investigation of reference 4.

Normal-shock rectangular, circular, and scoop inlets were tested. Figure 1 depicts these inlets and gives dimensions and station numbers. Figure 2 presents photographs of representative inlets for comparison. All inlets were sharp lipped (normal-shock lip angle is 8°) and, with the exception of configuration IX, each inlet incorporated a constant-area section approximately 3 inlet diameters long in order to maintain maximum pressure recovery (ref. 4). The normal-shock inlets, configurations I, II, V, and VI (figs. 1 and 2(b) and (e)), incorporated internal flow turning of 10° in the constant-area section between stations 1 and 2.

Configurations VII and VIII (figs. 2(c) and (d)) were external-compression inlets with wedge half-angles of 10°. These inlets were designed to operate adjacent to the boundary-layer generating surface ($I/\delta = 1.0$) and at a Mach number of 2.0. These inlets and configurations III and IV did not include flow turning. Configuration VIII differed from VII in that the wedge of configuration VIII was cut off at the point in the boundary layer where the oblique shock detached from the wedge.

The scoop inlet (configuration IX) pictured in figures 1 and 2(a) was designed to represent the simplest inlet that could be fabricated by stamping. It was meant to operate adjacent to the generating surface with a height approximately equal to that of the boundary layer.

The diffuser dimensions and angles for the inlets tested are tabulated in figure 1. Figure 2(f) pictures a diffuser-inlet combination with no turning installed for testing.

METHOD OF CALCULATION

A 1/9 power boundary-layer profile was used for all theoretical calculations. This equation,

$$\frac{u}{U_0} = \left(\frac{y}{\delta}\right)^{1/9}$$

is plotted in figure 3. Comparison of the theoretical profile with the experimentally surveyed profile (fig. 3) justifies its use. This profile is similar to that used in reference 4 and, therefore, permits comparison of data from reference 4 with the data in this report. The theoretical pressure recoveries and mass-flow ratios at critical operation can be calculated for normal-shock inlets using the method described in reference 5. This method involves a simplifying assumption that total temperature is constant through the boundary layer. An estimate of the resulting error showed the theoretical mass flows to be 1.5 percent too low for the worst case (small rectangular inlet adjacent to the surface at $M_0 = 2.0$).

For critical operation at design Mach number, the mass-flow ratios for the external-compression inlets (configurations VII and VIII) are the same as those for the normal-shock inlet of the same shape and area. In calculations of the theoretical pressure recoveries for the external-compression inlets, an area-weighted average of the local oblique-shock plus normal-shock recovery was used. The above theories were used in computing the values given in table I.

An approximate calculation of critical mass flow and pressure recovery was made for the normal-shock inlets using the stream-filament method of reference 1. For this calculation, a 1/9 power profile was substituted for the 1/7 power profile used in reference 1, and no diffuser total-pressure loss was assumed.

DISCUSSION OF RESULTS

Inlet maps with varying immersion ratios are presented in figure 4 for all configurations tested. Critical pressure recoveries and mass flows from these data are listed in table I for each combination of Mach number and immersion ratio.

In figure 5, the critical pressure recovery and mass-flow ratio of each inlet are plotted as functions of the centroidal immersion ratio $\overline{I}/\delta$. Also plotted for comparison are values of pressure recovery and mass flow calculated by the methods of references 1 and 5. As the inlets were immersed in the boundary layer, their recoveries and mass flows decreased in the manner described by the theory. For most configurations, the stream-filament method yielded values within 3 percent of the more exact calculation (ref. 5).

The experimental values fell below those calculated by an amount that increased with increased immersion and varied only slightly with stream Mach number (fig. 6). Pressure recovery varied from 95 to 80 percent of theoretical, and mass flow varied from 100 to 95 percent of theoretical as the inlets were immersed from the free stream to the boundary-layer generating surface. Larger errors were observed with the simple scoop (configuration IX). This inlet exhibited relatively low recovery because of its abrupt turning and poor internal diffusion. It exhibited relatively low mass flow at low Mach numbers ($M_0 = 1.3$) as a possible result of choking. The low mass-flow ratios exhibited (figs. 5(d) to (f)) by the external-compression inlets (configurations VII and VIII) do not necessarily indicate large deviation from theory, since no attempt was made to predict the oblique-shock spillage expected from such inlets at off-design speeds and immersion ratios.

To illustrate the effect of turning the flow, the pressure-recovery - mass-flow plots of figure 7 are presented. Superimposing the plot for rectangular inlets with 10° turning on that for no turning shows that the pressure recovery was decreased by only 0.03 at $I/\delta = 1.0$. Practically no effect is shown with the inlet operating in the free stream (figs. 7(a) and (b)). Comparison of configurations I and II (circular inlets, figs. 7(c) and (d)) to like configurations in reference 4 (figs. 7(c) and (g) of ref. 4) shows a 0.07 total-pressure loss for the small circular inlet (configuration I) at $I/\delta = 0.46$ and

M_0 = 2.0 and 1.5. A loss of approximately 0.02 is noted for the large circular inlet (configuration II) for like conditions.

The external-compression inlets (configurations VII and VIII) investigated showed little improvement over the simple normal-shock inlet when both were fully immersed in the boundary layer ($\overline{I}/\delta = 1$). Figure 8 superimposes the two external-compression-inlet performance maps on that of the normal-shock inlet at $I/\delta = 1.0$ and $M_0 = 2.0$. Critical pressure recoveries remained the same for all three inlets, while the critical mass flow decreased 0.07 for configuration VII. The mass flow for configuration VIII (short wedge) was 0.03 higher than that of the full-length wedge (configuration VII). This was to be expected because of the removal of the wedge at the shock detachment point in the boundary layer (see fig. 1, configuration VIII).

Distortion values for all configurations are presented in figure 9. The approximate average distortion at critical operation was 5 percent. A maximum distortion of 23 percent is shown for the scoop inlet (configuration IX).

Although the data are not shown, pressure fluctuations at the diffuser exit were approximately 3 percent of free-stream total pressure. The maximum fluctuation was 7 percent for configuration VII (external compression).

SUMMARY OF RESULTS

The internal performance of a series of circular and rectangular auxiliary air inlets was obtained at varying immersion heights in a turbulent boundary layer. The configurations were tested at Mach numbers of 1.3, 1.5, and 2.0. Results were as follows:

1. Experimental values of pressure recovery varied from 95 to 80 percent of theoretical, while mass flow varied from 100 to 95 percent of theoretical as the inlets were immersed in the boundary layer.

2. A simple calculation utilizing the centroid of the inlet area (stream-filament method) gave a good approximation of theoretical pressure recovery and mass flow.

3. Turning of the flow through an angle of 10° within the rectangular inlets decreased the inlet pressure recovery by a maximum of 0.03. In the case of the circular inlets, a decrease of 0.07 was noted for the small inlet.

4. In the cases tested, the use of external compression gave negligible improvement in inlet performance with the inlet fully immersed in the boundary layer.

5. Average distortion of the flow at critical operation for all inlets tested was approximately 5 percent.

Lewis Flight Propulsion Laboratory
National Advisory Committee for Aeronautics
Cleveland, Ohio, October 24, 1956

4184

REFERENCES

1. Hearth, Donald P., Englert, Gerald W., and Kowalski, Kenneth L.: Matching of Auxiliary Inlets to Secondary-Air Requirements of Aircraft Ejector Exhaust Nozzles. NACA RM E55D21, 1955.

2. Hearth, Donald P., and Cubbison, Robert W.: Investigation at Supersonic and Subsonic Mach Numbers of Auxiliary Inlets Supplying Secondary Air Flow to Ejector Exhaust Nozzles. NACA RM E55J12a, 1956.

3. Pennington, Donald B., and Simon, Paul C.: Internal Performance at Mach Numbers to 2.0 of Two Auxiliary Inlets Immersed in Fuselage Boundary Layer. NACA RM E53L28b, 1954.

4. Simon, Paul C.: Internal Performance of a Series of Circular Auxiliary-Air Inlets Immersed in a Turbulent Boundary Layer Mach Number Range: 1.5 to 2.0. NACA RM E54L03, 1955.

5. Simon, Paul C., and Kowalski, Kenneth L.: Charts of Boundary-Layer Mass Flow and Momentum for Inlet Performance Analysis - Mach Number Range, 0.2 to 5.0. NACA TN 3583, 1955.

TABLE I. - INLET TOTAL-PRESSURE RECOVERIES AND MASS-FLOW RATIOS AT CRITICAL OPERATION

Configuration	Free-stream Mach number, M_0	Immersion ratio, I/δ														
		Free stream					0.46					1.00				
		Centroidal immersion ratio, $\bar{I}/\delta$	Theory		Experiment		Centroidal immersion ratio, $\bar{I}/\delta$	Theory		Experiment		Centroidal immersion ratio, $\bar{I}/\delta$	Theory		Experiment	
			Total-pressure recovery, P_5/P_0	Mass-flow ratio, m/m_0	Total-pressure recovery, P_5/P_0	Mass-flow ratio, m/m_0		Total-pressure recovery, P_5/P_0	Mass-flow ratio, m/m_0	Total-pressure recovery, P_5/P_0	Mass-flow ratio, m/m_0		Total-pressure recovery, P_5/P_0	Mass-flow ratio, m/m_0	Total-pressure recovery, P_5/P_0	Mass-flow ratio, m/m_0
I	2.0	-----	0.72	1.00	----	----	0.24	0.88	0.94	0.81	0.94	0.78	0.44	0.68	0.57	0.69
	1.5	-----	.93	1.00	----	----	.24	.87	.96	.77	.97	.79	.65	.73	.55	.69
	1.3	-----	.98	1.00	----	----	.24	.94	.97	.78	.95	.79	.72	.76	.62	.74
II	2.0	-0.43	0.72	1.00	0.71	1.00	0.05	0.88	0.95	0.85	0.97	0.57	0.52	0.77	0.46	0.75
	1.5	-.43	.93	1.00	.88	1.00	.05	.88	.96	.85	.99	.57	.72	.82	.64	.80
	1.3	-.43	.98	1.00	.91	1.00	.05	.93	.96	.88	.96	.57	.79	.85	.68	.80
III	2.0	-0.14	0.72	1.00	0.69	1.00	0.32	0.86	0.93	0.82	0.94	0.86	0.40	0.62	0.33	0.82
	1.5	-----	.93	1.00	----	----	.32	.86	.96	.79	.95	.86	.66	.69	.51	.66
	1.3	-----	.98	1.00	----	----	----	.93	.96	----	----	----	.68	.71	----	----
IV	2.0	-0.28	0.72	1.00	0.71	1.00	0.18	0.88	0.96	0.84	0.94	0.75	0.47	0.71	0.39	0.69
	1.5	-.28	.93	1.00	.89	1.00	.18	.89	.97	.85	.96	.75	.68	.77	.58	.75
	1.3	-.28	.98	1.00	.95	1.00	.18	.95	.98	.86	.93	.75	.75	.79	.65	.73
V	2.0	-0.14	0.72	1.00	0.71	1.00	0.32	0.86	0.94	0.81	0.90	0.86	0.41	0.65	0.51	0.82
	1.5	-.14	.93	1.00	.90	1.00	.32	.88	.97	.76	.94	.86	.62	.70	.49	.86
	1.3	-.14	.98	1.00	.91	1.00	----	.94	.98	----	----	----	.69	.75	----	----
VI	2.0	-0.28	0.72	1.00	0.71	1.00	0.18	0.88	0.96	0.84	0.92	0.75	0.47	0.71	0.39	0.87
	1.5	-.28	.93	1.00	.91	1.00	.18	.89	.97	.82	.96	.75	.68	.77	.55	.72
	1.3	-.28	.98	1.00	.93	1.00	.18	.95	.98	.86	.93	.75	.75	.79	.63	.73
VII	2.0	-0.28	----	----	0.73	0.96	0.18	----	----	0.70	0.90	0.75	0.52	0.70	0.38	0.82
	1.5	-.28	----	----	.94	.90	.18	----	----	.81	.85	.75	----	----	.58	.81
	1.3	-.28	----	----	.95	.84	.18	----	----	.86	.78	.75	----	----	.64	.81
VIII	2.0	-----	----	----	----	----	0.18	----	----	0.88	0.90	0.75	0.52	0.70	0.40	0.85
	1.5	-----	----	----	----	----	.18	----	----	.85	.88	.75	----	----	.58	.82
	1.3	-----	----	----	----	----	.18	----	----	.86	.81	.75	----	----	.64	.84
IX	2.0	-----	----	----	----	----	----	----	----	----	----	0.81	0.51	0.75	0.51	0.76
	1.5	-----	----	----	----	----	----	----	----	----	----	.81	.68	.79	.53	.76
	1.3	-----	----	----	----	----	----	----	----	----	----	.81	.77	.81	.62	.68

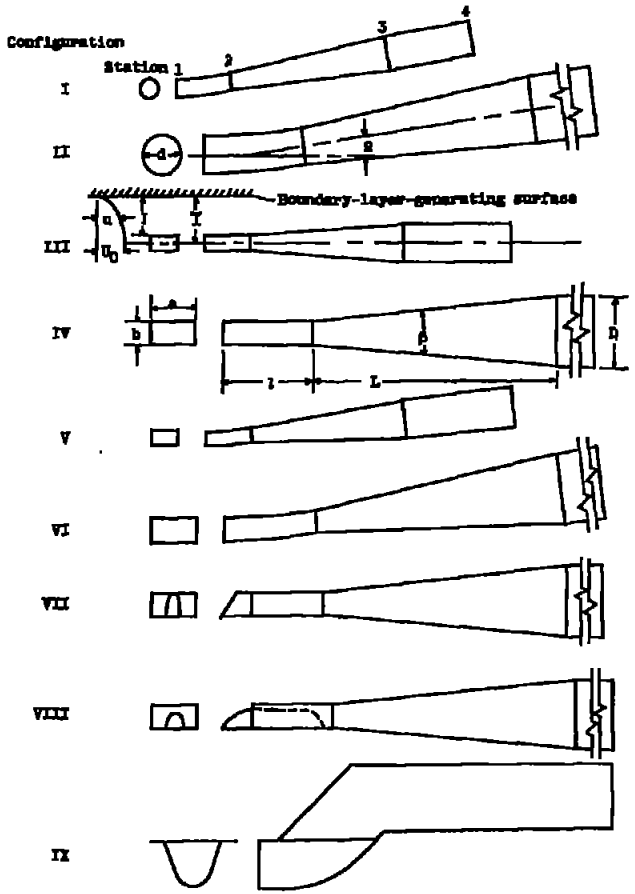

Configuration	Inlet width, a, in.	Inlet height, b, in.	Inlet diameter, d, in.	Diffuser-exit inside diameter, D, in.	Length of constant-area section, l, in.	Length of diffuser conical section, L, in.	Conical-diffuser included angle, β, deg	Flow turning angle, α, deg
I	——	——	2	3.78	5.46	15.70	8.5	10
II	——	——	4	7.56	10.91	31.41	8.5	10
III	2.55	1.27	——	3.78	4.80	16.34	8.2	0
IV	5.10	2.55	——	7.56	9.60	32.72	8.2	0
V	2.55	1.27	——	3.78	4.77	16.34	8.2	10
VI	5.10	2.55	——	7.56	9.54	32.72	8.2	10
VII	5.10	2.55	——	7.56	11.1	32.72	8.2	0
VIII	5.10	2.55	——	7.56	12.35	32.72	8.2	0
IX	8.00	4.65	4	8.00	13.31	38.31	——	45

Figure 1. - Configurations tested.

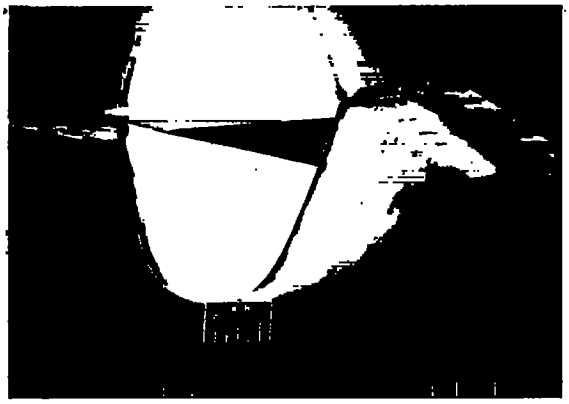

(a) Configuration IX; scoop.

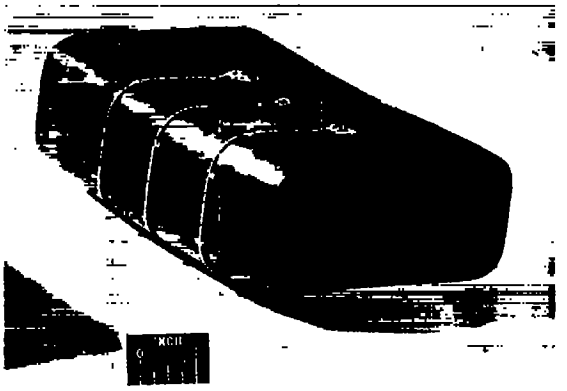

(b) Configuration VI; large, rectangular, curved.

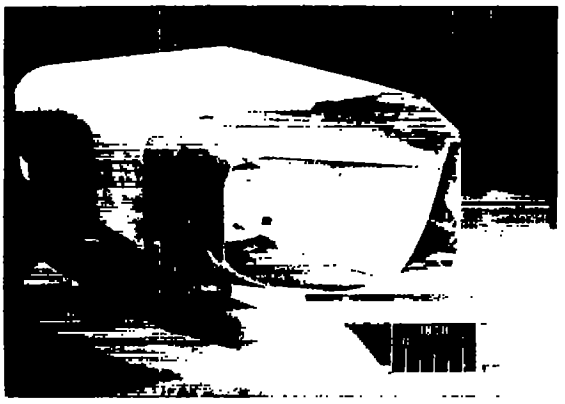

(c) Configuration VII; external-compression, rectangular.

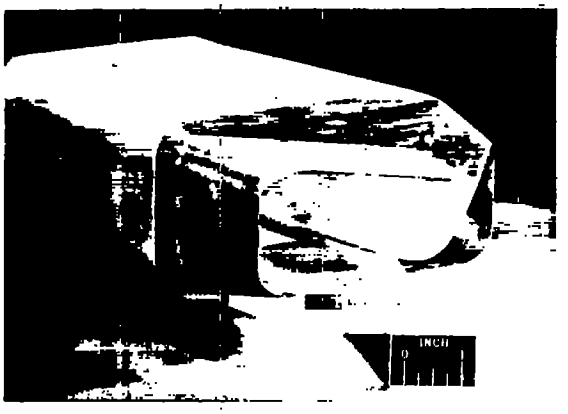

(d) Configuration VIII; external-compression, rectangular, short-wedge.

(e) Configuration II; large, circular, curved.

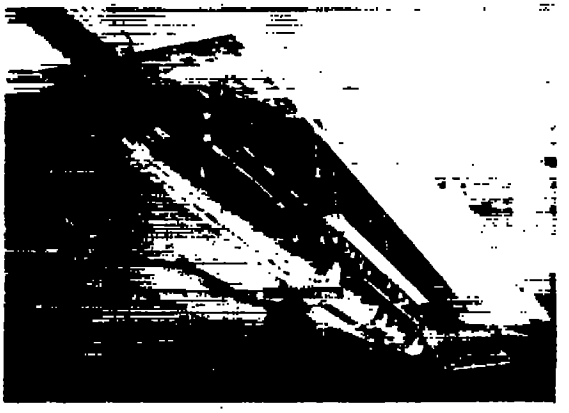

(f) Installation detail; no turning.

C-45265

Figure 2. - Model installation and representative inlets.

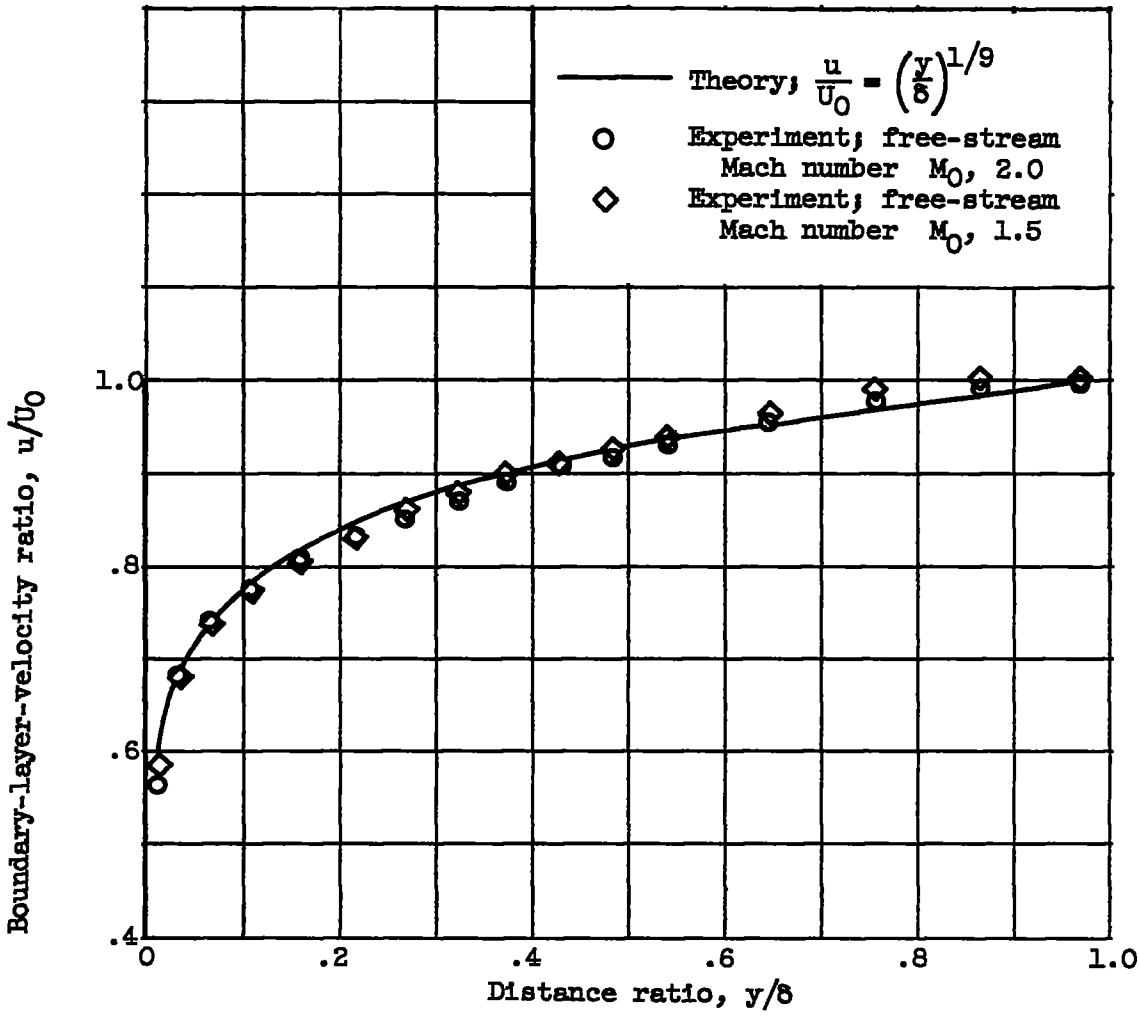

Figure 3. - Boundary-layer profiles ahead of inlet (inlet not present).

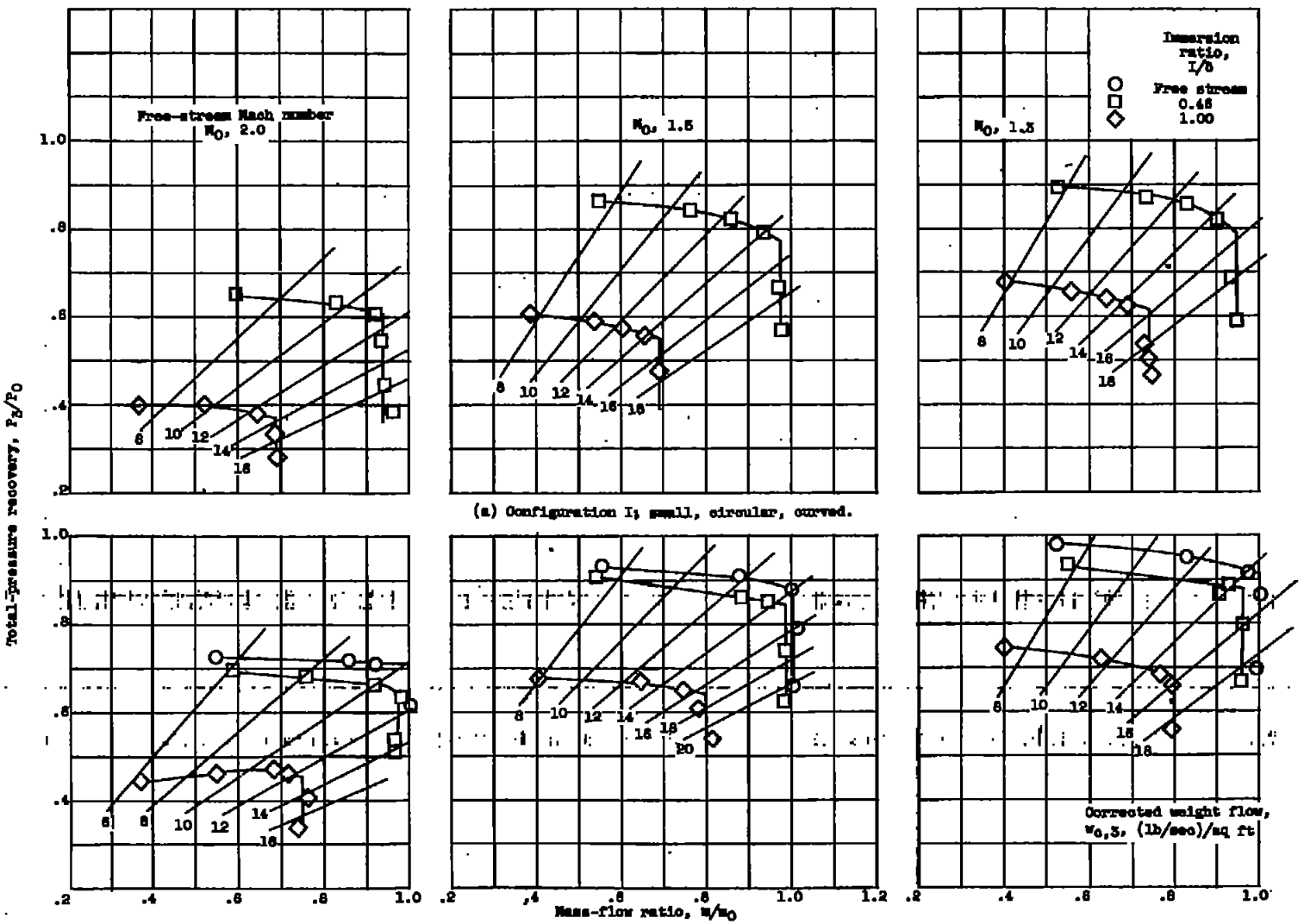

(a) Configuration I; small, circular, curved.

(b) Configuration II; large, circular, curved.

Figure 4. - Inlet performance characteristics.

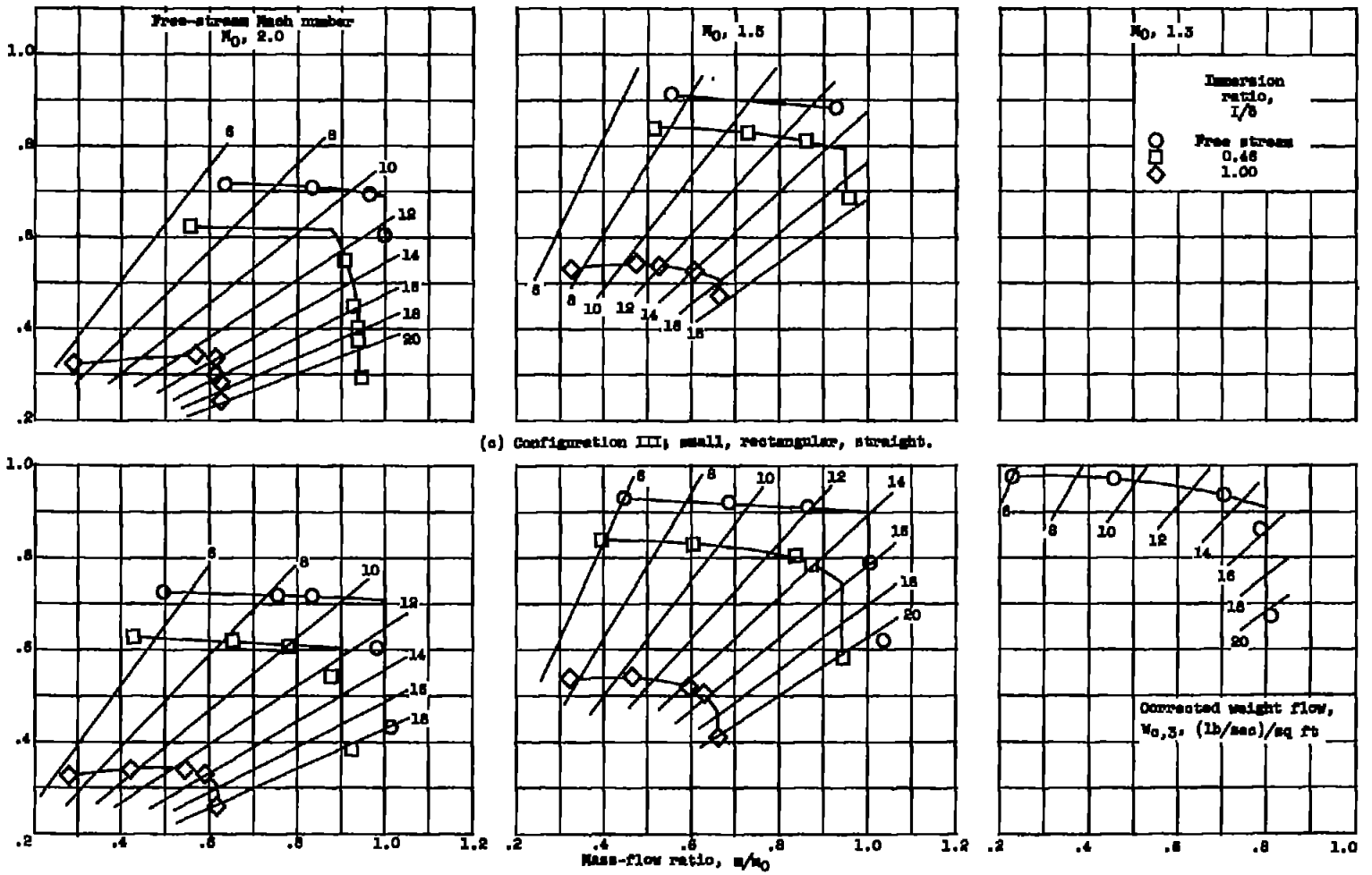

(c) Configuration III; small, rectangular, straight.

(d) Configuration V; small, rectangular, curved.

Figure 4. - Continued. Inlet performance characteristics.

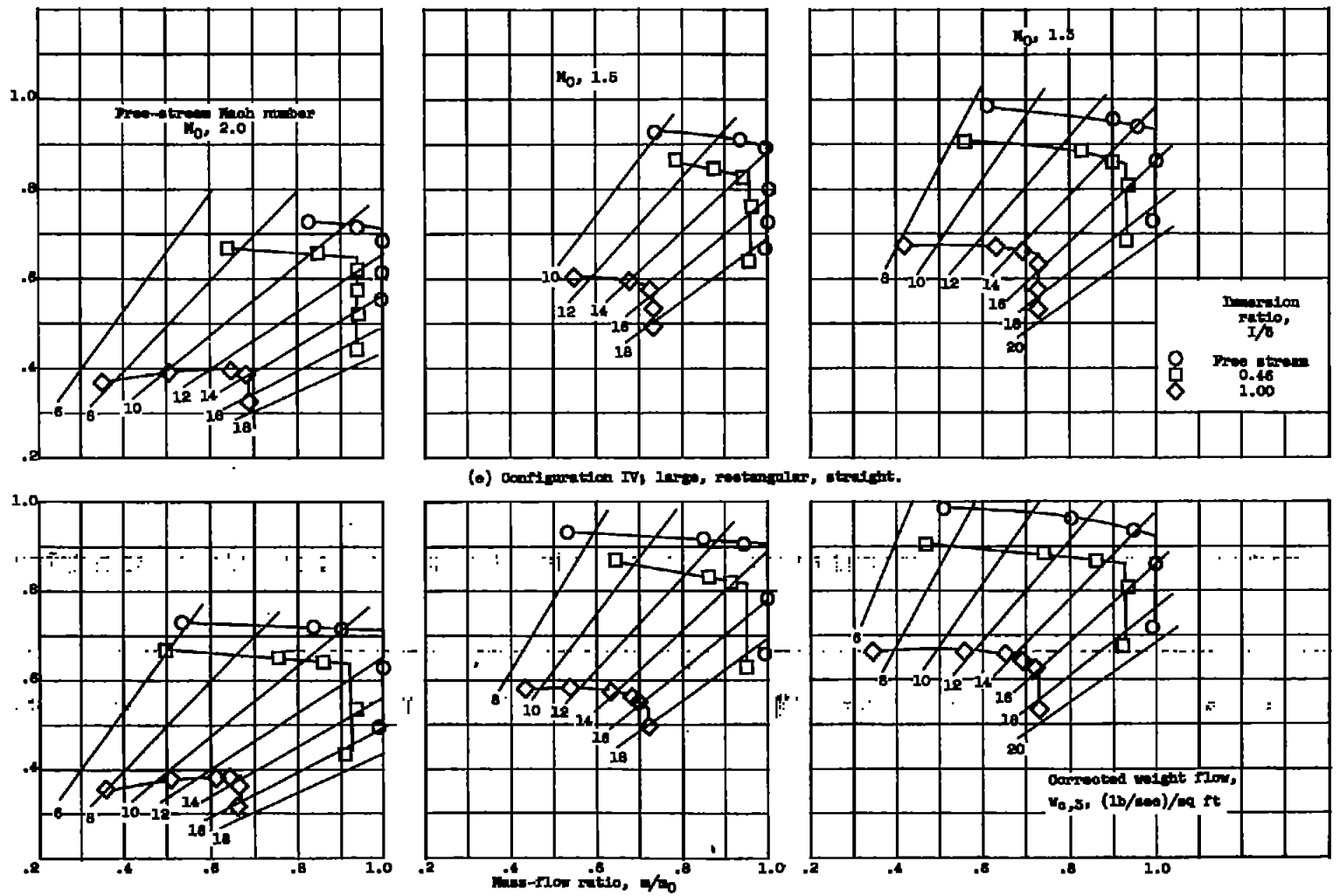

(e) Configuration IV; large, rectangular, straight.

(f) Configuration VI; large, rectangular, curved.

Figure 4. - Continued. Inlet performance characteristics.

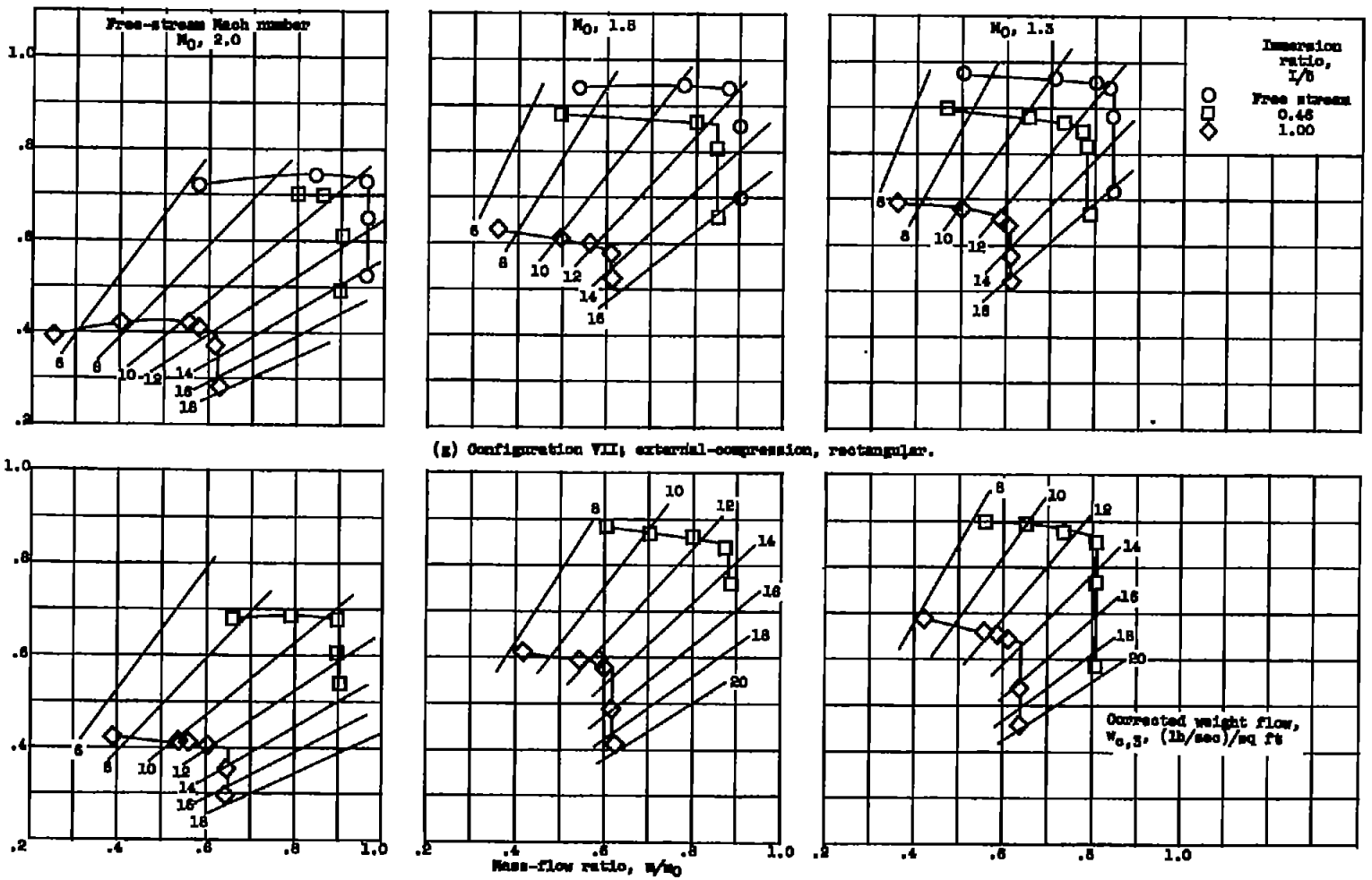

(g) Configuration VII; external-compression, rectangular.

(h) Configuration VIII; external-compression, rectangular, short-wedge.

Figure 4. - Continued. Inlet performance characteristics.

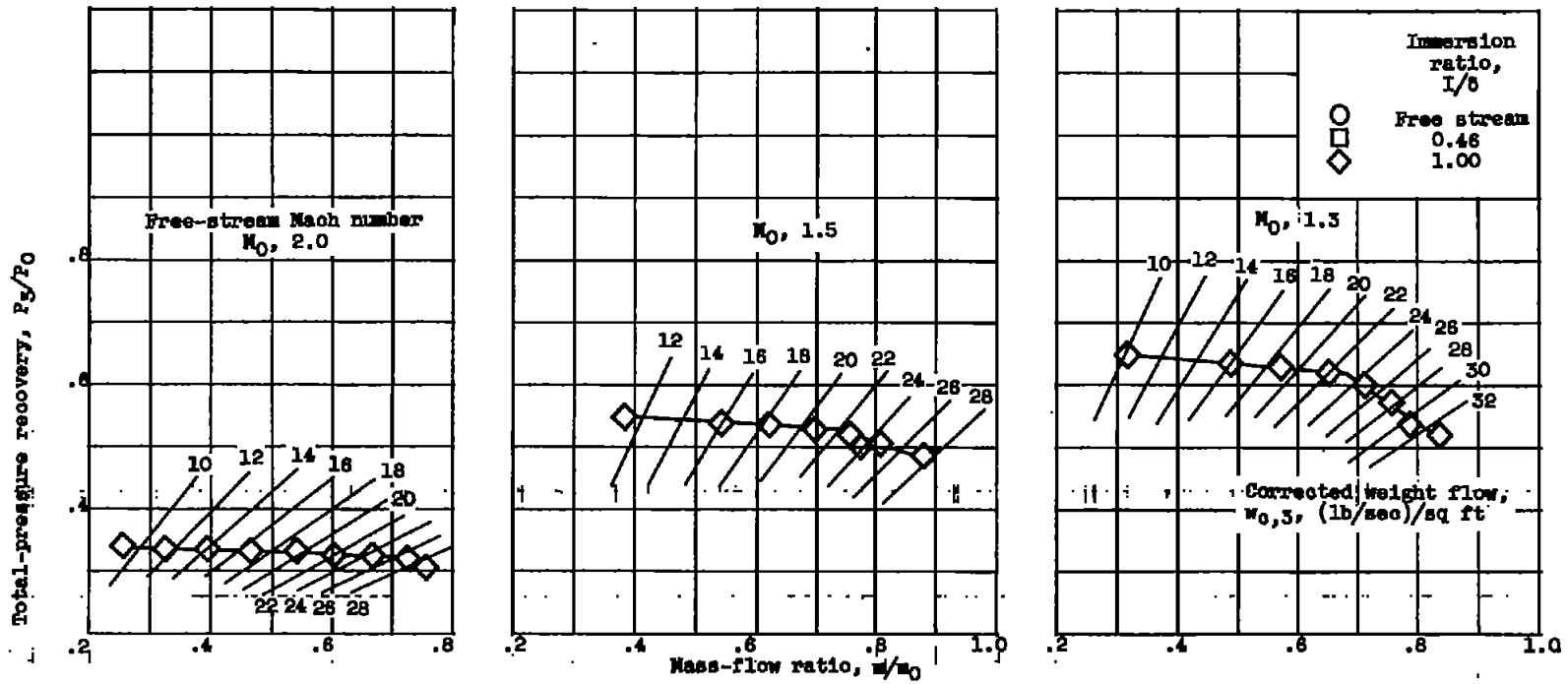

(i) Configuration IX; scoop.

Figure 4. - Concluded. Inlet performance characteristics.

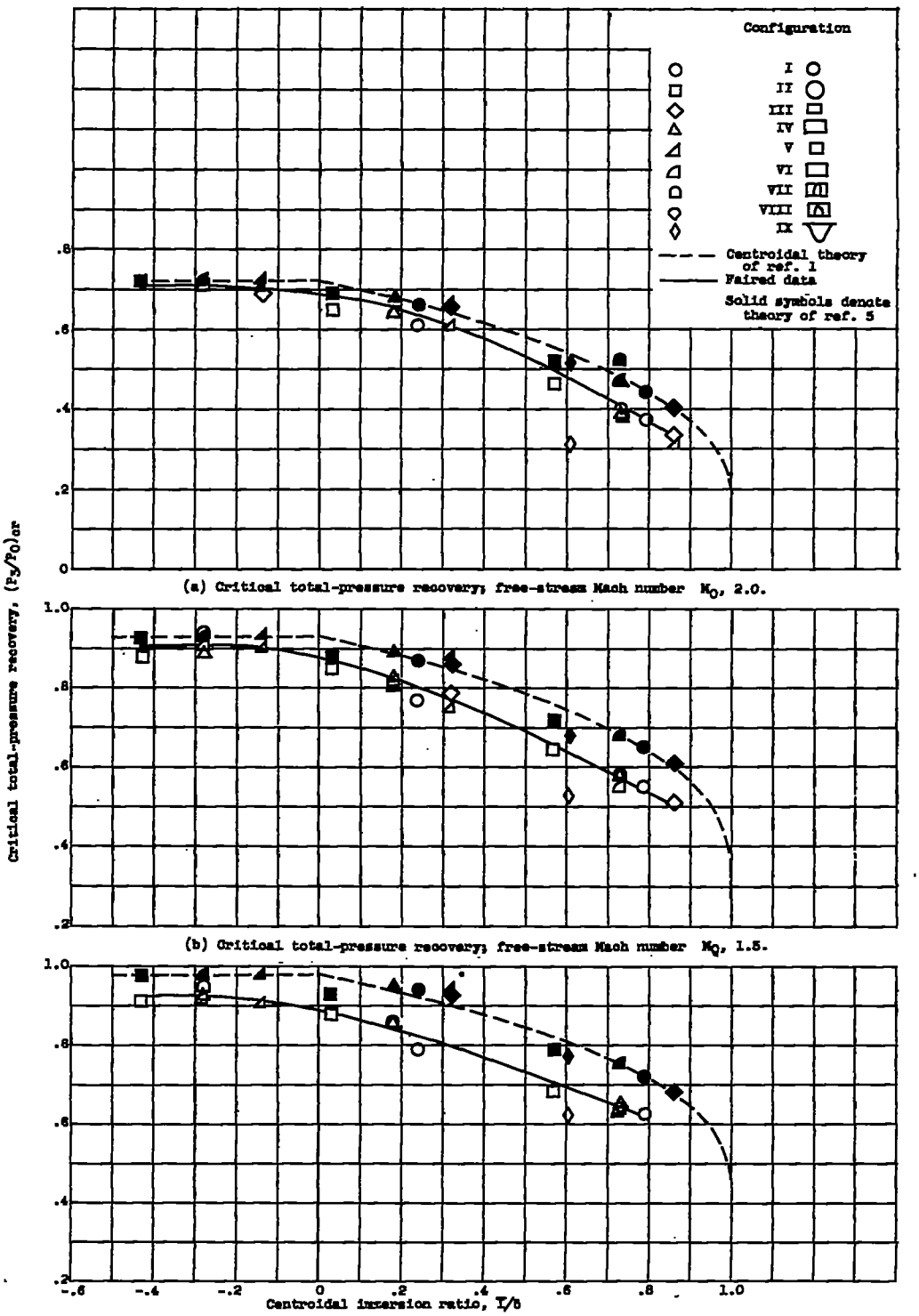

Figure 5. - Correlation of effect of inlet immersion on critical pressure recovery and mass-flow ratio with theory of reference 5.

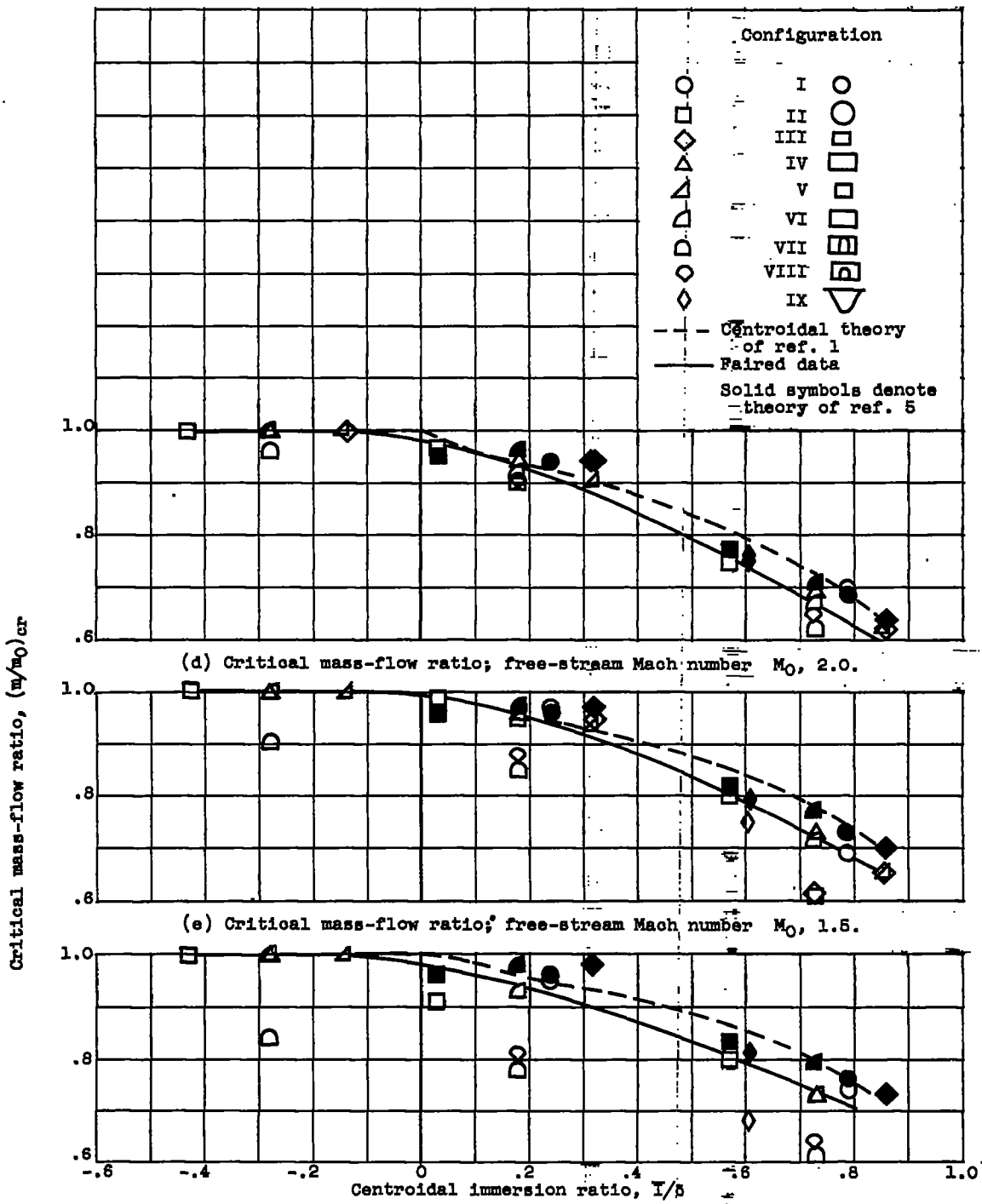

(d) Critical mass-flow ratio; free-stream Mach number M_0, 2.0.

(e) Critical mass-flow ratio; free-stream Mach number M_0, 1.5.

(f) Critical mass-flow ratio; free-stream Mach number M_0, 1.3.

Figure 5. - Concluded. Correlation of effect of inlet immersion on critical pressure recovery and mass-flow ratio with theory of reference 5.

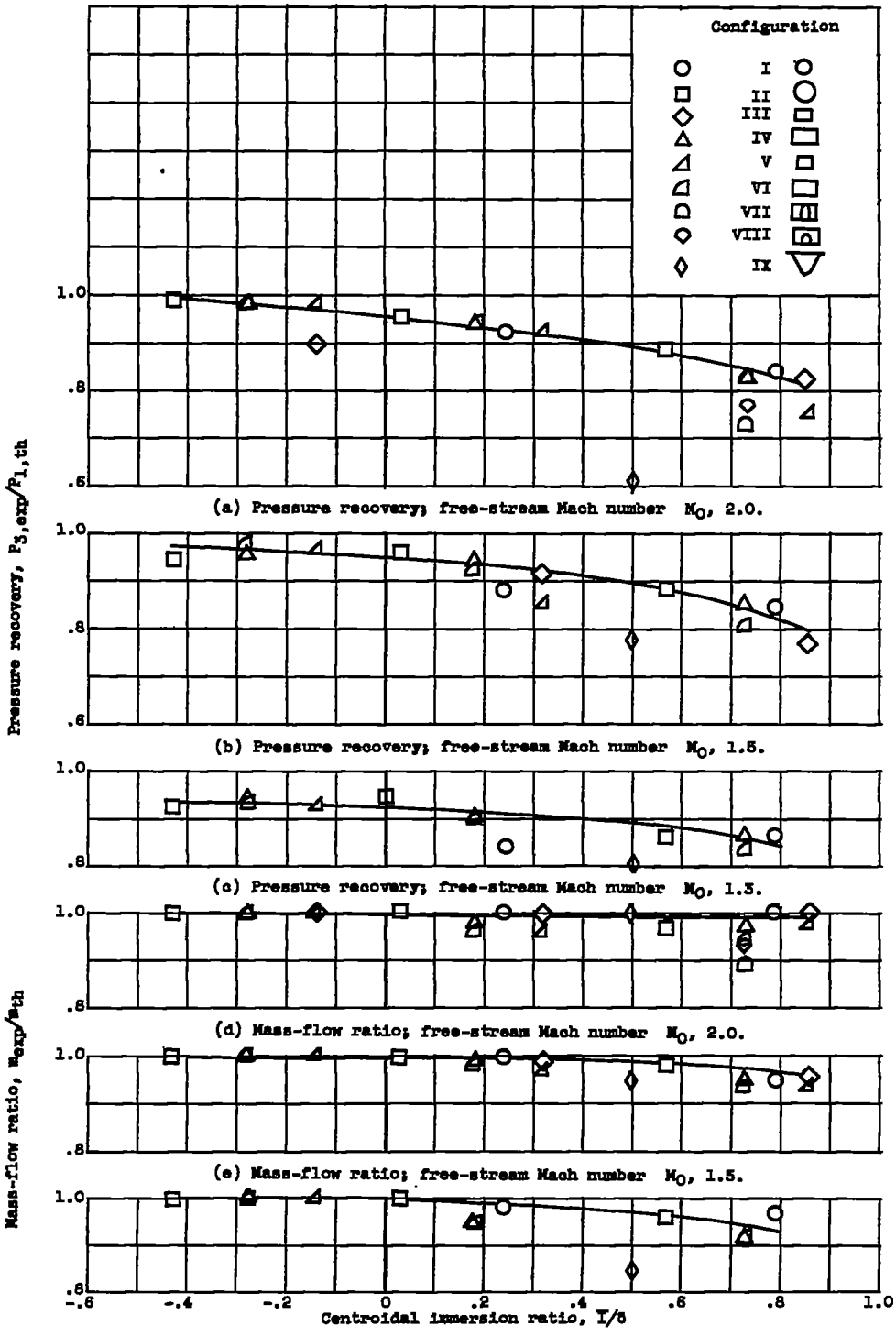

(a) Pressure recovery; free-stream Mach number M_0, 2.0.

(b) Pressure recovery; free-stream Mach number M_0, 1.5.

(c) Pressure recovery; free-stream Mach number M_0, 1.3.

(d) Mass-flow ratio; free-stream Mach number M_0, 2.0.

(e) Mass-flow ratio; free-stream Mach number M_0, 1.5.

(f) Mass-flow ratio; free-stream Mach number M_0, 1.3.

Figure 6. - Ratio of experimental to theoretical critical pressure recovery and mass-flow against centroidal immersion ratio.

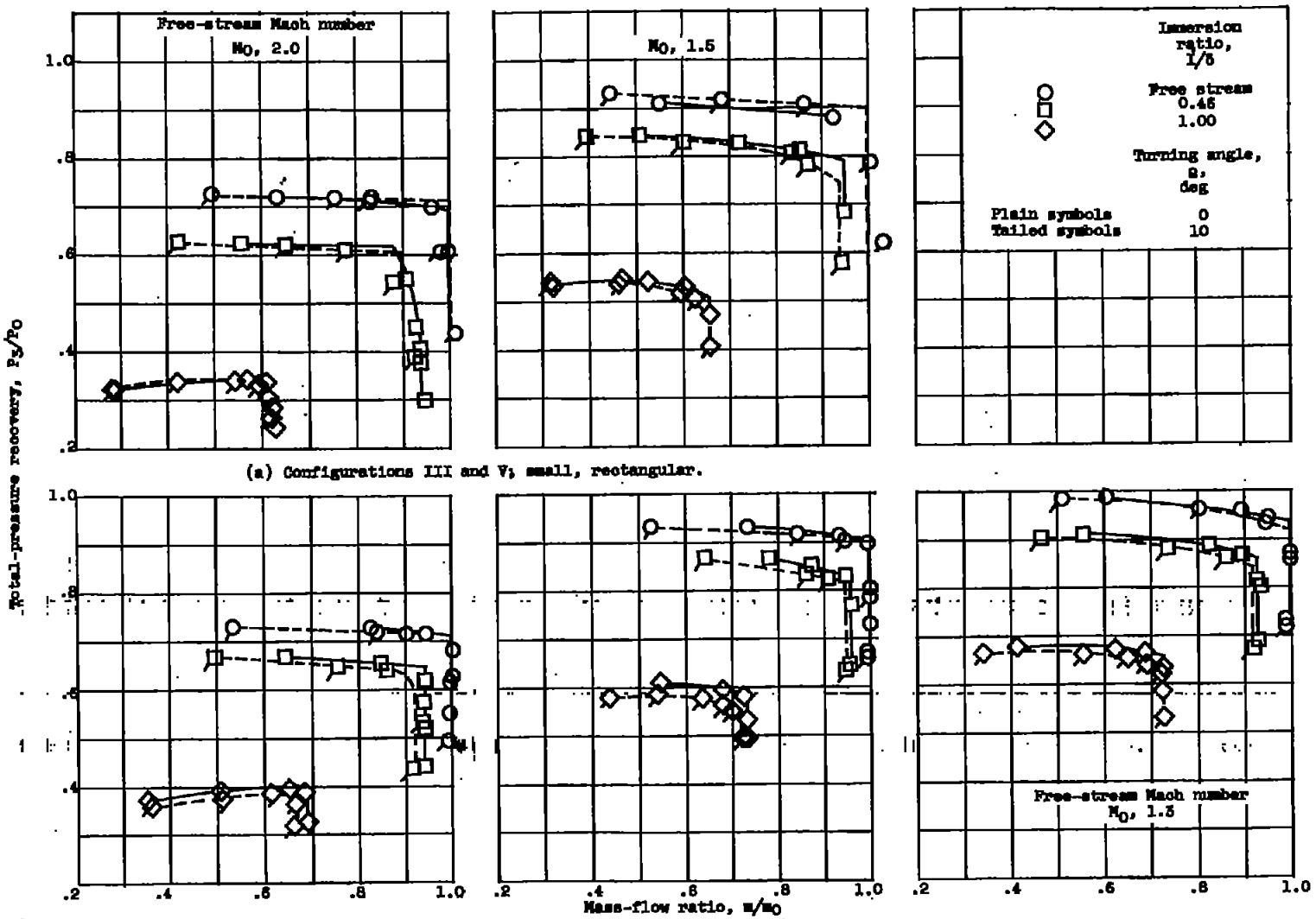

(a) Configurations III and V; small, rectangular.

(b) Configurations IV and VI; large, rectangular.

Figure 7. - Effect of flow turning in diffuser.

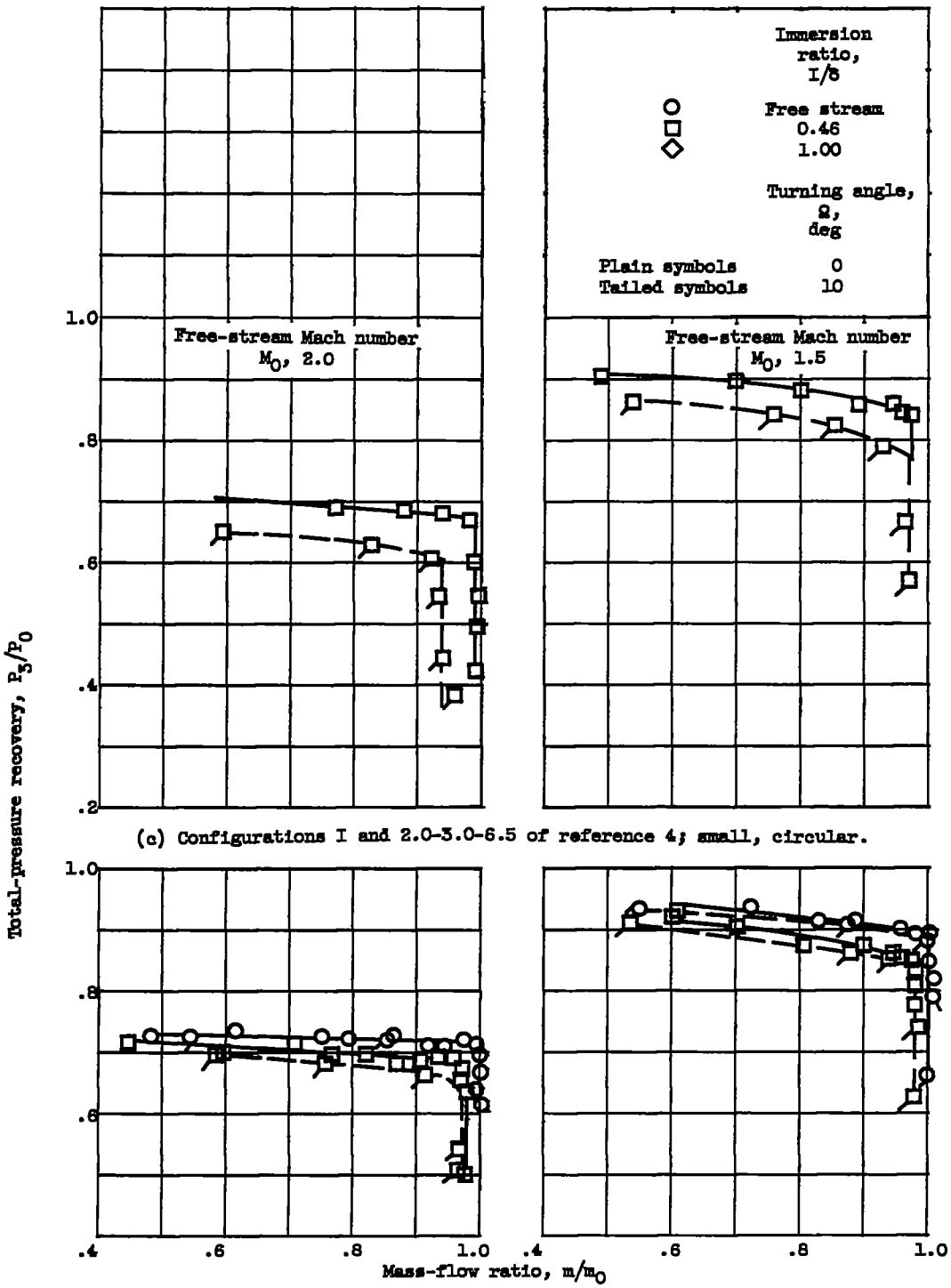

(c) Configurations I and 2.0-3.0-6.5 of reference 4; small, circular.

(d) Configurations II and 4.0-3.0-6.5 of reference 4; large, circular.

Figure 7. - Concluded. Effect of flow turning in diffuser.

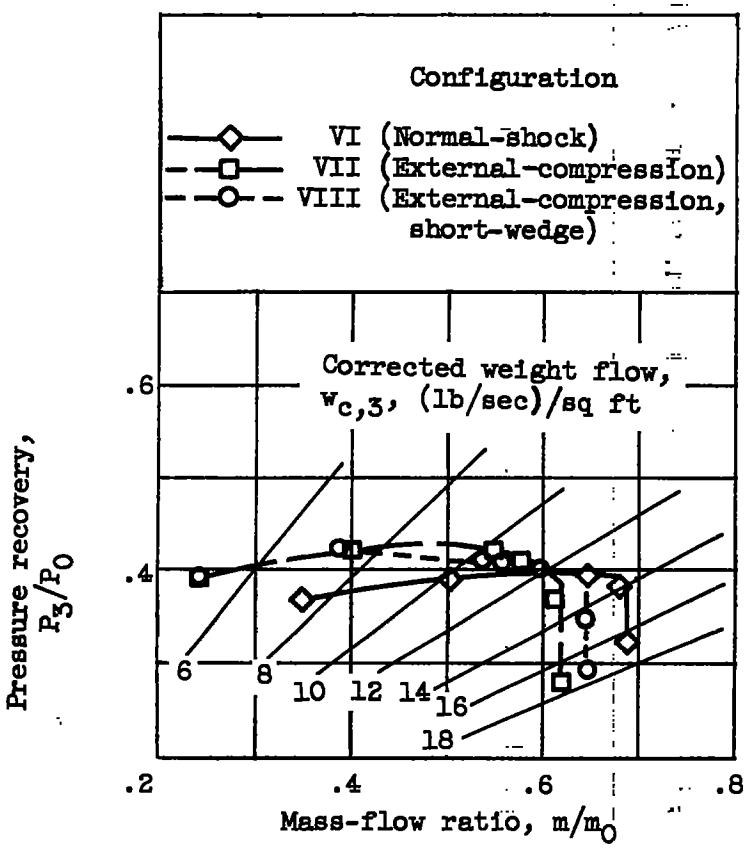

Figure 8. - Comparison of normal-shock with external-compression inlets. Free-stream Mach number M_0, 2.0; immersion ratio I/δ, 1.0.

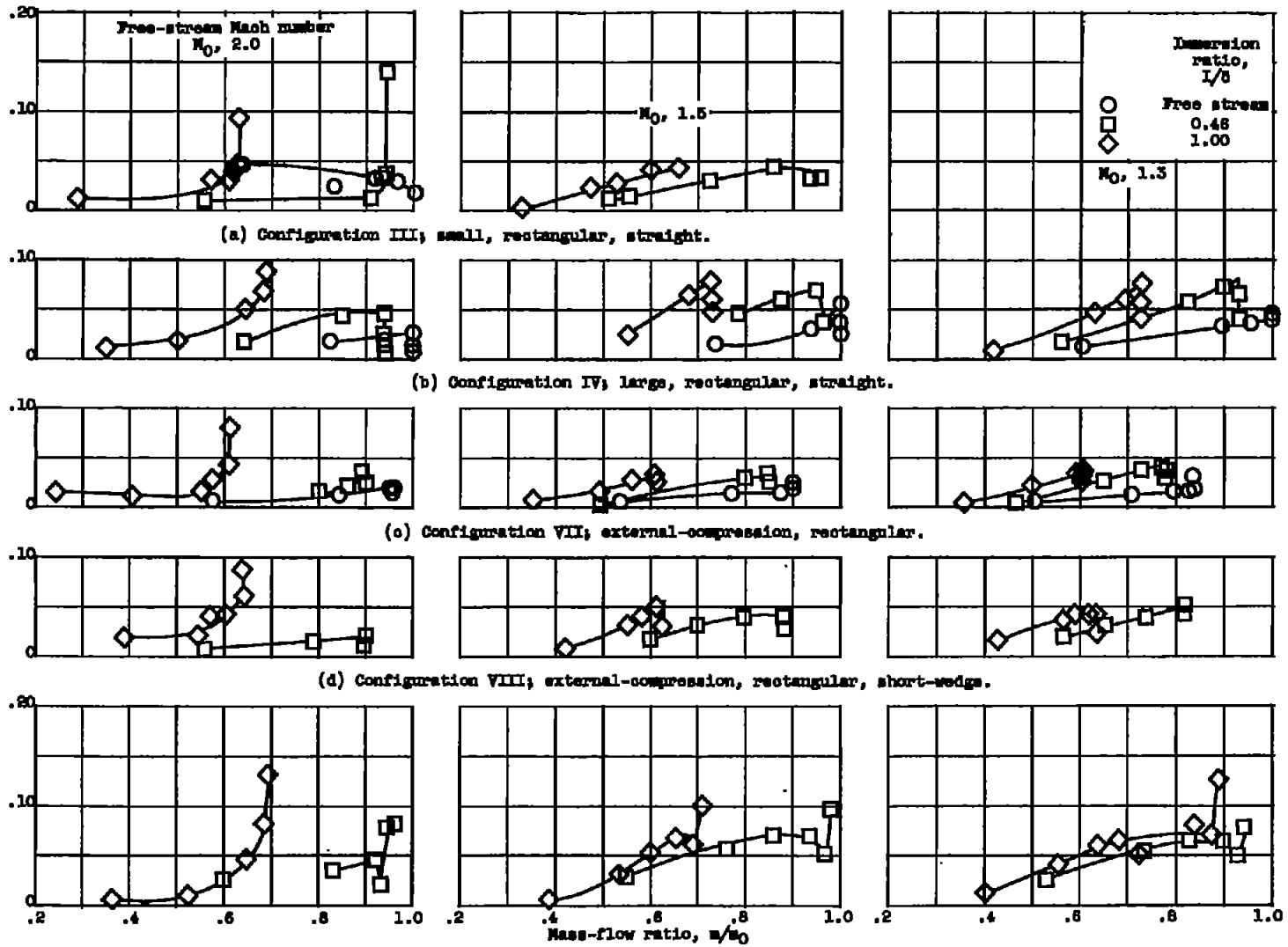

(a) Configuration III; small, rectangular, straight.

(b) Configuration IV; large, rectangular, straight.

(c) Configuration VII; external-compression, rectangular.

(d) Configuration VIII; external-compression, rectangular, short-wedge.

(e) Configuration I; small, circular, curved.

Figure 9. - Distortion at diffuser exit.

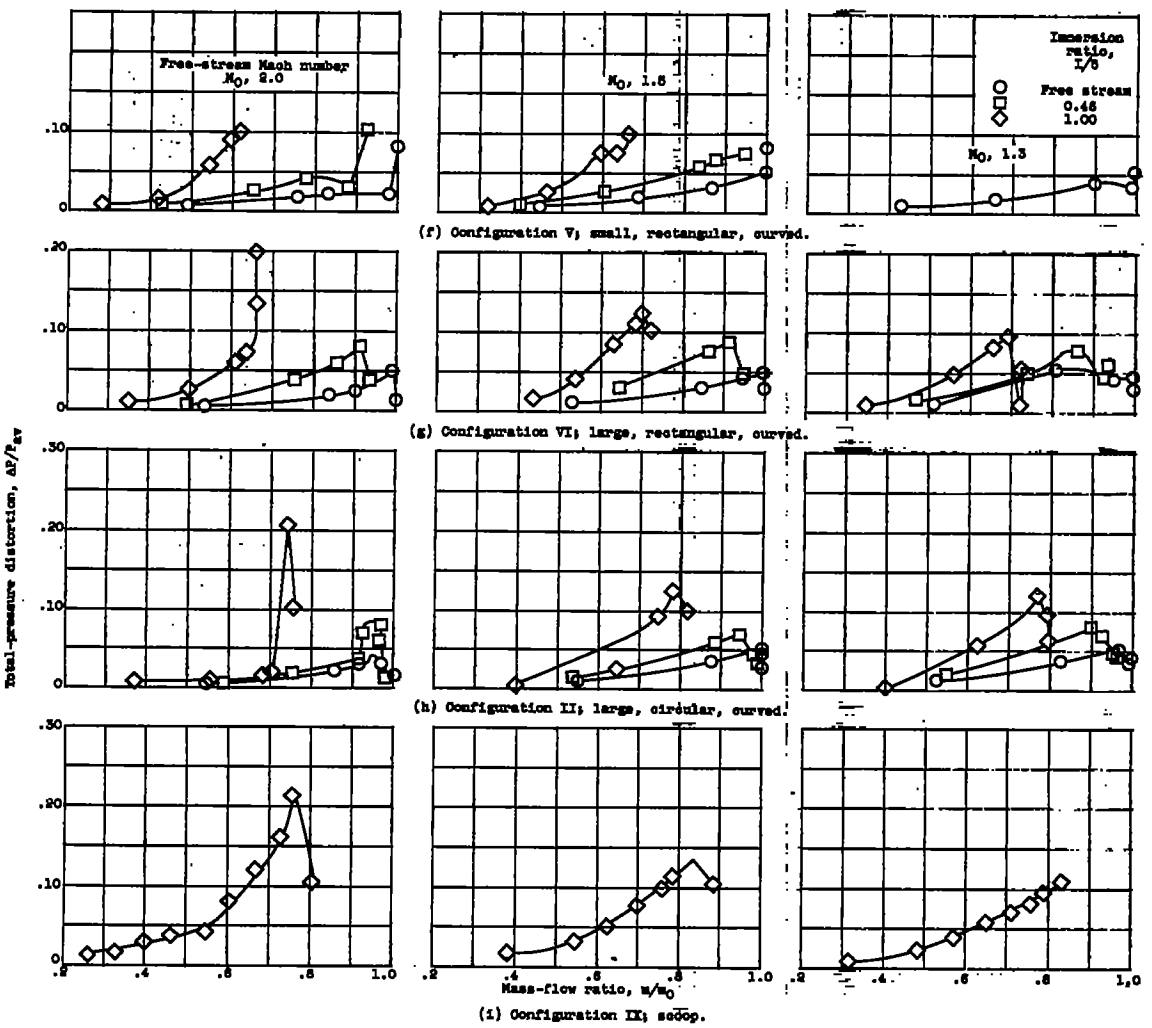

Figure 9. - Concluded. Distortion at diffuser exit.